Journal of Oceanology and Limnology

https://doi.org/10.1007/s00343-026-5501-1

Research Paper

FCRS-Mamba: a fine-scale remote sensing classification method for coral reef geomorphology based on an omnidirectional selective scanning strategy*

Wenshuo ZHU[1, 2, 3, 7], Guangbo REN[2, 3], Yabin HU[2, 3, **], Feifei ZHANG[2, 3, 4], Yi MA[2, 3, 7], Qiuhua TANG[1, 2], Qi SHI[5], Hongliang MENG[6], Bo AI[1]

[1] *College of Geodesy and Geomatics, Shandong University of Science and Technology, Qingdao 266590, China*

[2] *First Institute of Oceanography, Ministry of Natural Resources, Qingdao 266061, China*

[3] *Technology Innovation Center for Ocean Telemetry, Ministry of Natural Resources, Qingdao 266061, China*

[4] *College of Oceanography and Space Informatics, China University of Petroleum, Qingdao 266500, China*

[5] *South China Sea Institute of Oceanology, Chinese Academy of Sciences, Guangzhou 510301, China*

[6] *Shandong Twenty First Century Aerospace Information Technology Co., Ltd., Yantai 264000, China*

[7] *National Engineering Laboratory for Integrated Aero-Space-Ground-Ocean Big Data Application Technology, Xi' an 710072, China*

Received Dec. 10, 2025; accepted in principle Jun. 1, 2026; accepted for publication Jun. 24, 2026

Abstract Coral reefs are among the most important ecosystems in the ocean, and achieving fine-scale geomorphic classification is essential for ecological conservation and resource management. However, the complexity, diversity, and stratified nature of reef geomorphic structures, together with heterogeneity arising from variations in water depth, continue to challenge conventional classification approaches. To address these limitations, this study introduces FCRS-Mamba, a fine-scale coral reef geomorphic classification model designed around an omnidirectional selective scanning strategy. The model incorporates an eight-direction Omnidirectional Selective Scan Module (OSSM) as its central component to effectively extract spatial features from high-resolution reef remote sensing imagery across multiple directions. Classification experiments were conducted on Antelope Reef and North Reef using imagery from the Beijing-3A (BJ-3A) and GF-2 satellites. FCRS-Mamba achieved an mIoU of 81.49% for fifteen geomorphic categories on Antelope Reef and 77.43% for nine categories on North Reef. Compared with existing approaches, it improved the average mIoU by 7.24% and 10.95% on Antelope Reef and North Reef, respectively. With its high classification accuracy, the model provides reliable data for coral reef ecological monitoring and marine resource management, thereby supporting ecological restoration planning, protected area delineation, and the advancement of sustainable marine ecosystem development.

Keyword: coral reef; geomorphic classification; remote sensing; state space model (SSM); semantic segmentation

1 INTRODUCTION

As one of the most structurally complex, biodiverse, and productive ecosystems on Earth (Bajjouk et al., 2019), coral reefs exhibit pronounced spatiotemporal heterogeneity in their geomorphic morphology. This complex geomorphic configuration not only supports a wide range of marine habitats but also plays a crucial role in sustaining fisheries resources, protecting coastal zones, and promoting the development of ecological tourism (Chan et al., 2024). However, under the

* Supported by the National Key Research and Development Program of China (No. 2022YFC3105100), the China High-Resolution Earth Observation System Program (No. 41-Y30F07-9001-20/22), the Shandong Provincial Natural Science Foundation (No. ZR2023MD073), and the National Natural Science Foundation of China (No. 42376185)

** Corresponding author: huyabin@fio.org.cn

combined pressures of climate warming and anthropogenic disturbances, coral reef ecosystems are undergoing unprecedented functional decline (Li et al., 2024a). In this context, establishing large-scale assessment frameworks for coral reef health has become an urgent priority for developing management strategies that mitigate degradation and enhance ecosystem resilience (Bajjouk et al., 2019). Within these efforts, geomorphic classification serves as a foundational element of coral reef health diagnostics. It provides essential support for advancing ecological conservation theory and facilitates the sustainable development of reef-based tourism through ecological-economic synergies.

Remote sensing is an essential tool for monitoring coral reef geomorphology, and existing approaches can be broadly categorized into manual interpretation and automated image classification. Manual interpretation relies heavily on expert knowledge and is inherently inefficient, which has driven increasing interest in automated classification methods. Current classification techniques include both traditional machine learning and deep learning techniques. In coral reef geomorphology studies, commonly used traditional machine learning methods include pixel-based classifiers such as maximum likelihood (ML) (Hochberg and Atkinson, 2003; Zou et al., 2006; Hu et al., 2010), support vector machines (SVM) (Gapper et al., 2019; Wicaksono et al., 2019; Pang et al., 2021; Wan et al., 2023), random forest (RF) (Wicaksono et al., 2019; Wan et al., 2023; Ji et al., 2024), K-Nearest Neighbor (KNN) (Wan et al., 2023), and XGBoost (Wan et al., 2023). Object-based image analysis (OBIA) has also been widely applied (Roelfsema et al., 2013; Gong et al., 2014; Zhang, 2015; Roelfsema et al., 2018, 2021; Hedley et al., 2018). However, most previous studies rely on satellite data such as IKONOS, Landsat 8, and Sentinel-2, whose spatial resolutions are generally below 10 m. This limits the number of identifiable geomorphic categories and makes small-scale geomorphic features difficult to detect, thereby constraining fine-scale classification. In addition, pixel-based classifiers typically overlook spatial and contextual relationships among pixels, whereas OBIA relies heavily on manually designed features and expert prior knowledge. These limitations, compounded by high computational complexity and limited generalization capability, hinder their effectiveness in complex coral reef geomorphic environments.

As an important branch of machine learning, deep learning has increasingly become a preferred approach for coral reef geomorphic classification due to its capacity to automatically learn hierarchical features from data. Representative models include ResNet152 and DeepLab v2 (King et al., 2018), CNN-SVM (Wan and Ma, 2020), Dense U-Net (Li et al., 2020), PRNet (Dong, 2021), U-Net (Dang et al., 2022), mRES-uNet (Giles et al., 2023), GCU-Net (Zhang, 2023; Zhang et al., 2024), and RTDL (Ai et al., 2024). Among them, GCU-Net introduces the Convolutional Block Attention Module (CBAM) into the U-Net architecture to construct the CU-Net framework for coral reef geomorphic classification and further incorporates a geospatial cognition module to post-process the initial classification results, thereby improving classification accuracy. Traditional CNN-based deep learning methods extract image features by stacking convolutional operations, which enables the effective capture of fine-grained local contextual information. However, their inherently limited receptive fields constrain the modeling of global context, making it difficult to fully learn complex semantic representations. In coral reef geomorphic classification, such CNN-based models can delineate large-scale geomorphic boundaries accurately but often struggle to capture overall scene semantics, spatial relationships among features, and the complete semantic layout of the scene. These limitations reduce classification accuracy for small-scale geomorphic features. Transformer-based models, in contrast, can theoretically model long-range dependencies more effectively than conventional CNNs and better capture global contextual information. A representative example is UNetFormer (Wang et al., 2022), which integrates Transformer and U-Net architectures to combine global contextual information with local spatial details, thereby improving semantic segmentation performance in remote sensing imagery. However, the relatively high computational complexity and memory consumption of Transformer models limit their operational efficiency, making them less practical for coral reef geomorphic classification and consequently hindering their widespread adoption in this field.

In recent years, the Mamba model (Gu and Dao, 2024) has received considerable attention in remote sensing image segmentation. Its core component, the state space model (SSM) (Gu et al., 2022), provides strong capabilities for capturing global contextual features and has served as the foundation for a series of semantic segmentation models, including Vim (Zhu et al., 2024), VMamba (Liu et al., 2024), RSM (Zhao et al., 2024), Pan-Mamba (He et al., 2024), RSMamba (Chen et al., 2024), RS3Mamba (Ma et al., 2024), PP-Mamba (Hu et al., 2024), Samba (Zhu et al., 2024), VM-Unet (Ruan et al., 2024), and MambaHSI (Li et al., 2024). Among these models, VM-Unet incorporates the Vision Mamba architecture into the U-Net framework, enhancing global contextual information modeling and long-range dependency representation through the SSM. MambaHSI further extends the Mamba architecture to hyperspectral remote sensing image segmentation tasks. Coral reef geomorphic categories differ markedly in spectral properties, textural patterns, and spatial scales, resulting in pronounced spatial heterogeneity and high feature complexity in high-resolution remote sensing imagery. These characteristics pose significant challenges for fine-scale classification. The Mamba architecture offers significant advantages in global feature extraction, making it highly promising for fine-scale coral reef geomorphic classification. However, several limitations remain when applying Mamba models to this task:

1) Existing Mamba models primarily rely on horizontally bidirectional scanning SSMs or four-directional scanning (SS2D) along both horizontal and vertical axes for global feature extraction. This approach limits their ability to fully capture the highly heterogeneous spatial distribution of coral reef geomorphic categories and often overlooks subtle features of small-scale reef units.

2) The encoder architectures of current Mamba models generally struggle to balance multi-scale and local information, restricting their capacity to comprehensively extract multi-level features of coral reef geomorphology.

3) The decoder designs of existing Mamba models are relatively simple and insufficiently integrate global and local contextual information across multiple scales, thereby constraining improvements in fine-scale classification performance for coral reef geomorphic categories.

To address the aforementioned limitations, this study proposes a four-layer dual-encoder remote sensing classification model for coral reef geomorphology, named FCRS-Mamba, which is built upon an omnidirectional selective scanning strategy. In this model, an auxiliary encoder based on the Omnidirectional Selective Scan Module (OSSM) captures multi-scale global contextual information, while the main encoder employing ResNet modules extracts multi-scale local features. A Collaborative Completion Module (CCM) is incorporated into the main encoder to enhance and fuse multi-scale features from both encoders. The decoder adopts a UNetFormer structure capable of jointly capturing global and local contextual information, thereby enabling fine-scale classification of coral reef geomorphic categories. Experiments were conducted on Antelope Reef and North Reef using 0.5-m high-resolution BJ-3A and 4-m GF-2 satellite imagery. Coral reef geomorphic labels were generated based on field measurements to validate the model. The main contributions of this study are summarized as follows:

1) A dual-encoder model, FCRS-Mamba, is proposed for fine-scale classification of coral reef geomorphology. The model demonstrates superior performance in classification tasks on Antelope Reef and North Reef, achieving average mIoU improvements of 7.24% and 10.95% over comparison models, respectively.

2) An OSSM with eight-direction global feature scanning capability is developed. By extending feature searches to diagonal and anti-diagonal directions, OSSM enhances the extraction of small-scale and diverse coral reef geomorphic features, improving separability among different geomorphic categories.

3) A CCM coupled with a lightweight, hierarchical decoder is constructed to achieve efficient multi-scale feature fusion. The CCM integrates global features from the auxiliary encoder with local features extracted by the main encoder (ResNet18), compensating for limitations in global feature extraction. The decoder incorporates a Global-Local Attention (GLA) mechanism, enabling balanced extraction of multi-scale global and local contextual features for high-accuracy, efficient fine-scale classification of coral reef geomorphic categories.

2 MATERIAL AND DATASET

2.1 Study area and data

The primary study area is Antelope Reef (Fig. 1), a ring-shaped atoll in the Yongle Atoll of the Xisha Islands, China. Positioned at 16°27′N and 111°35′E, the reef covers approximately 15 km². A small sand cay, Kuangzai Sand Cay, with an area of 0.01 km², is located on the southeastern side of the reef

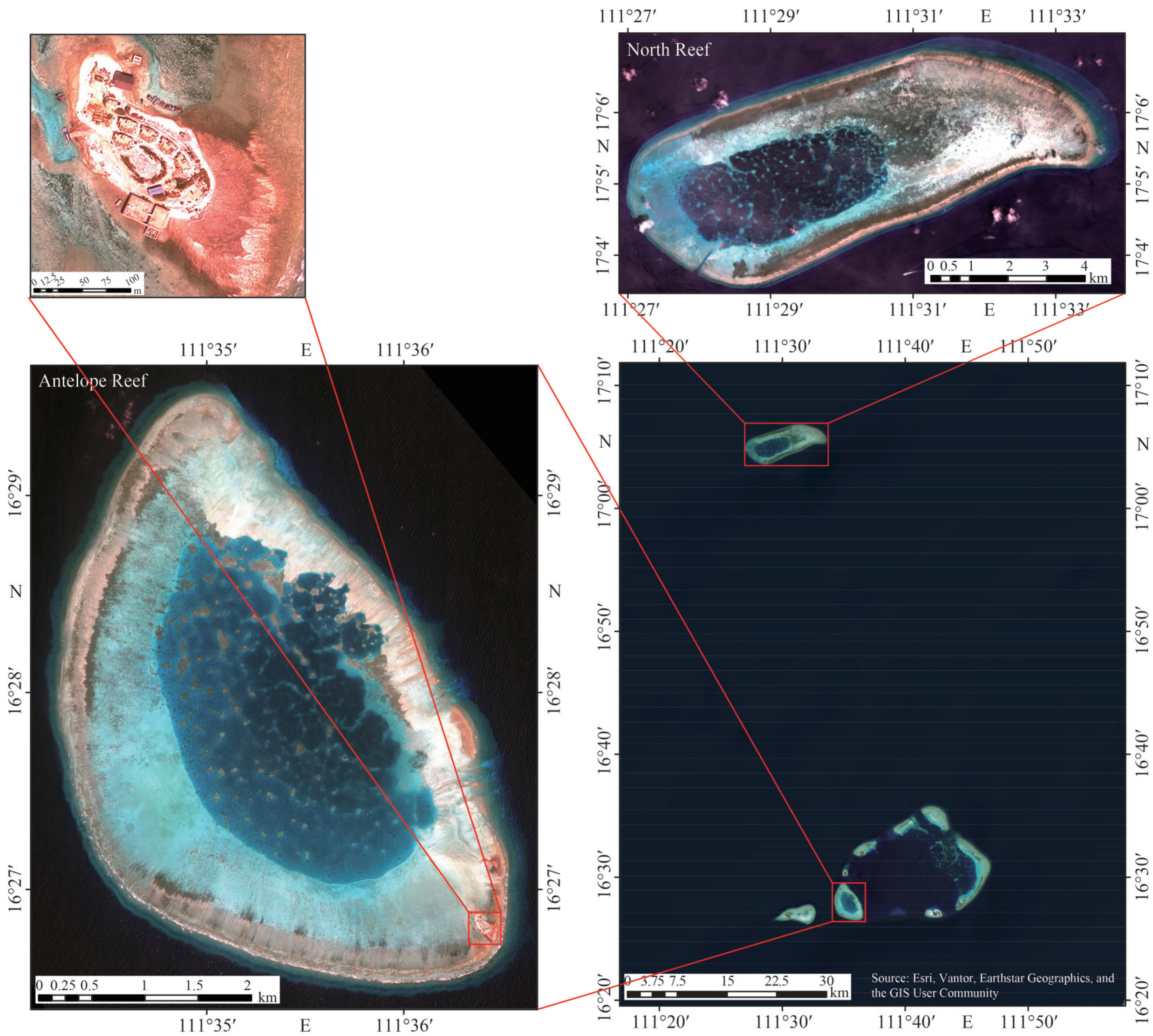

Fig.1 The images of the study areas

platform. Data for this area was obtained from the BJ-3A satellite (Table 1). The imagery used corresponds to the Antelope Reef area captured on March 5, 2024. After fusion of the panchromatic and multispectral bands, a multispectral image with a spatial resolution of 0.5 m was generated, comprising 11 536×14 337 pixels.

The second study area is North Reef, a submerged coral reef located at the northernmost tip of the Xisha Islands, China (17°05′N, 111°30′E), covering approximately 50 km^2. A true-color image of the reef is shown in Fig.1. Data for this area was obtained from the GF-2 satellite, with detailed specifications provided in Table 1. This multispectral imagery used in this study was acquired on September 13, 2020, with a spatial resolution of 4 m

Table 1 Detailed parameters of the satellites

Parameter	BJ-3	GF-2
Launch time	June 11, 2021	August 19, 2014
Spatial resolution	Panchromatic: 0.5 m, Multispectral: 2 m	Panchromatic: 0.8 m, Multispectral: 3.2 m
Swath width	≥23 km (dual camera)	45 km (dual camera)
Spectral band	Panchromatic: 450–700 nm Multispectral: blue: 450–520 nm, green: 520–590 nm, red: 630–690 nm, NIR: 770–890 nm	Panchromatic: 450–900 nm Multispectral: blue: 450–520 nm, green: 520–590 nm, red: 630–690 nm, NIR: 770–890 nm
Orbit type	Sun-synchronous orbit	Sun-synchronous orbit
Orbit altitude	500 km	631 km
Revisit cycle	3–5 d (one satellite)	5 d
Design lifetime	8 years	5–8 years

and a size of 3 192×1 753 pixels.

Field investigations were conducted in the Xisha Islands in 2013, 2015, and 2019, during which in-situ coral reef geomorphological data were collected from 138 survey stations. Of these, 23 stations were located on Antelope Reef and 11 on North Reef. A schematic diagram showing the in-situ data is presented in Fig.2.

2.2 Classification system

The classification system used in this study is based on the fine-scale coral reef geomorphology framework proposed by Zhang (2023), which comprises 26 geomorphic categories. Building upon this system, visual interpretation identified 14 geomorphic categories in Antelope Reef, including deep fore-reef slope (DFS), shallow fore-reef slope (SFS), reef crest (RC), algal reef (AR), sparse coral-depositional area (SCA), dense coral-depositional area (DCA), reef-clumping area (RA), lagoon (L), lagoon pinnacle patch reef (LPPR), lagoon flat patch reef (LFPR), beach (B), sandbar (S), vegetation (V), and man-made structure area (MSA). An additional deep water (DW) category was introduced, resulting in a total of 15 geomorphic categories for Antelope Reef.

In this study, the Deep Water category generally refers to marine areas located beyond the coral reef system. These areas typically have water depths greater than 15 m, where seafloor geomorphic information cannot be reliably identified from remote sensing imagery. As a result, these regions cannot be confidently assigned to specific coral reef geomorphic categories and were therefore treated as an independent Deep Water category.

In contrast, North Reef contains 9 geomorphic categories, including DW, SFS, RC, DCA, RA, L, LPPR, LFPR, and tidal channel (TC). These differences reflect substantial variation in geomorphological composition between Antelope Reef and North Reef.

2.3 Experimental sample setting

Guided by expert knowledge and in-situ data, visual interpretation was applied to classify the geomorphic categories of 15 subareas within Antelope Reef, collectively referred to as Sample 1. In addition, 10 elongated east-west transect samples were specifically designed across Antelope Reef and defined as Sample 2. To meet the requirements for model training and testing, Samples 1 and 2 were divided into a training set and a test set at a ratio of 4:1. Sample 3 was constructed by combining sub-samples selected from both Sample 1 and Sample 2, and it was used to evaluate different label selection strategies as discussed in Section 5.2. During the division of Sample 3 into training and test sets, the principle of maintaining a consistent number of pixels was strictly followed. Accordingly, Samples 2–6 were selected instead of Samples 1–8 and 1–10, and pixels were allocated in a 4:1 ratio. Sample 1 and Sample 2 correspond to Fig.3a and Fig.3b, respectively. Detailed sample settings are provided

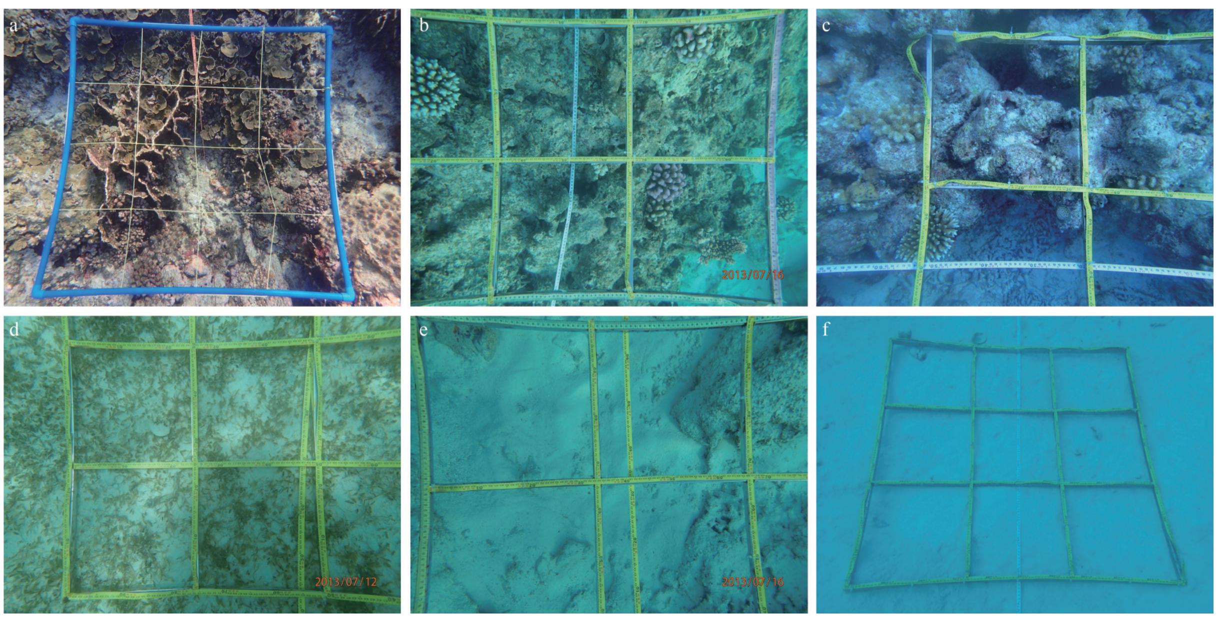

Fig.2 In-situ coral reef geomorphological data from Antelope Reef and North Reef

a. reef-clumping area; b. shallow fore-reef slope; c. deep fore-reef slope; d. algal reef; e. sparse coral-depositional area; f. lagoon.

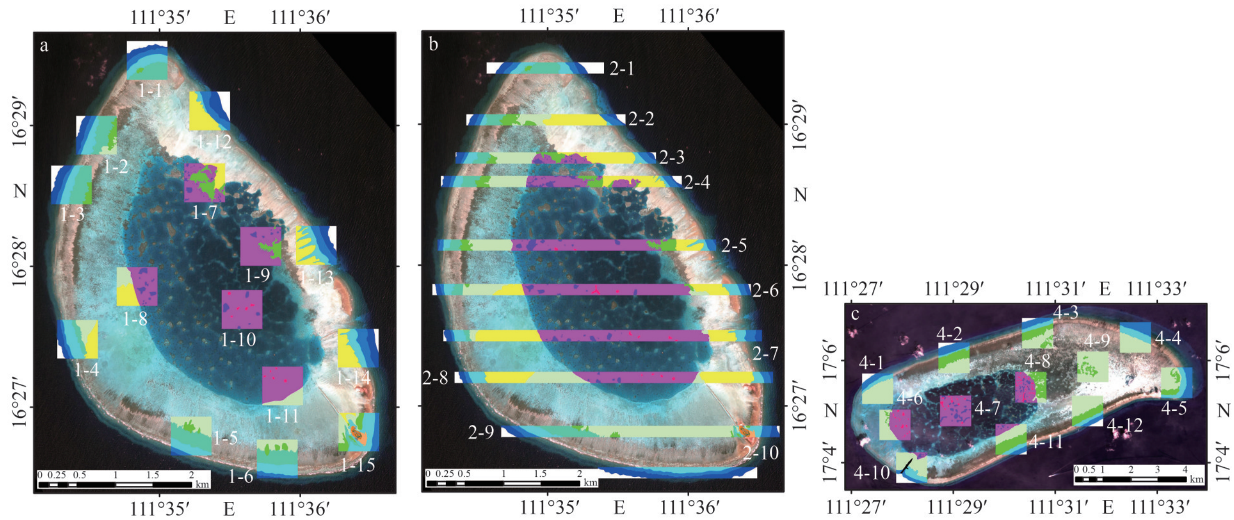

Fig.3 The schematic of sample selection

a. Sample 1 of Antelope Reef; b. Sample 2 of Antelope Reef; c. Sample 4 of North Reef.

in Table 2.

The spatial resolution of the North Reef data is 4 m, compared with 0.5 m for Antelope Reef. This difference requires that each North Reef sample cover a larger area while meeting the same sample size constraints. Because this study focuses on algorithm comparison, the sample selection strategy for North Reef differs from that used for Antelope Reef to ensure both sufficient sample volume and representative spatial coverage. Instead of employing elongated strip-shaped samples across the reef, 12 independently distributed samples were selected, as shown in Fig.3c, and these were further divided into a training set and a test set in a ratio of 3:1.

To ensure the reliability of the geomorphic samples, visual interpretation was conducted under the guidance of expert knowledge and in-situ survey data, which provided important references for geomorphic category identification and boundary delineation. The interpreted geomorphic categories at the in-situ survey locations were consistent with the corresponding field records. In addition, class separability analysis was performed using samples extracted from the visual interpretation results. The average separability values were 1.88 for Antelope Reef and 1.89 for North Reef, indicating high overall separability among geomorphic categories.

3 METHODOLOGY

The FCRS-Mamba model retains the basic structure of RS3Mamba and is composed of the Omnidirectional Selective Scanning (OSS) auxiliary encoder, the Residual main encoder with CCM, and the UNetFormer decoder, as shown in Fig.1. The model adopts a dual-branch architecture in which the main encoder and the auxiliary encoder independently extract features from coral reef remote sensing images. Each branch contains four hierarchical modules. The features extracted at each layer of the auxiliary encoder are deeply fused with the corresponding features from the main encoder through the CCM module. After four layers of feature extraction and cross-encoder fusion, the resulting multi-scale features are transmitted to the decoder through skip connections to generate the final predictions. The model is trained using the cross-entropy loss function.

Table 2 Experimental sample settings

Study area	Sample name	Training sample	Test sample
Antelope Reef	Sample 1	1-1, 1-2, 1-3, 1-4, 1-6, 1-7, 1-8, 1-10, 1-11, 1-12,1-14, 1-15	1–5, 1–9, 1–13
	Sample 2	2-1, 2-3, 2-4, 2-6, 2-7, 2-8, 2-9, 2-10	2–2, 2–5
	Sample 3	1-1, 1-2, 1-3, 1-4, 1-6, 1-7, 1-11, 1-12, 1-14, 1-15, 2-6	1–5, 1–9, 1–13
North Reef	Sample 4	4-1, 4-3, 4-4, 4-5, 4-7, 4-8, 4-9, 4-10, 4-12	4–2, 4–6, 4–11

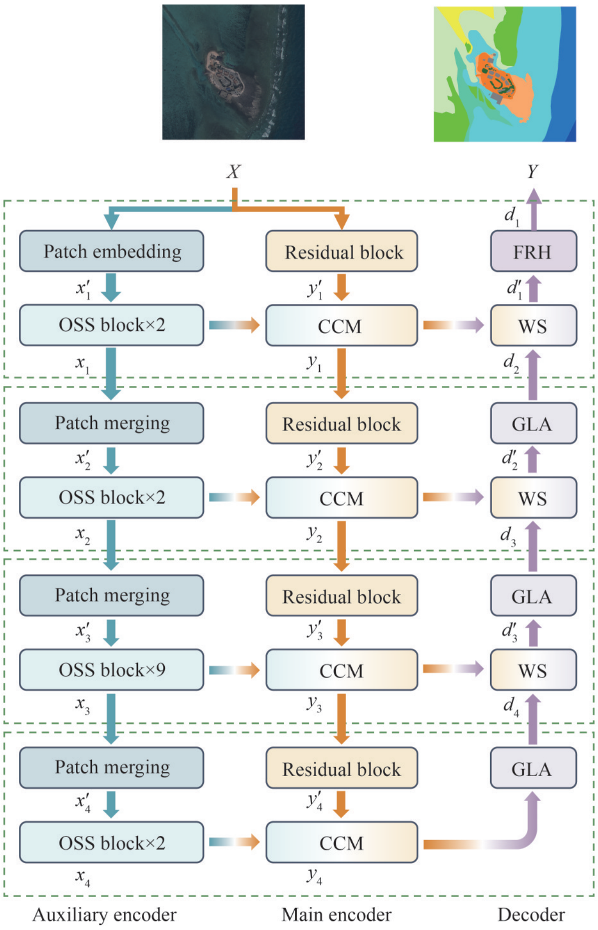

Fig.4 The overall architecture of FCRS-Mamba

3.1 OSS auxiliary encoder

The OSS auxiliary encoder functions as the global-context branch of the FCRS-Mamba model, responsible for capturing long-range contextual information. In coral reef geomorphic classification, geomorphic units such as lagoons, coral-depositional zones, and fore-reef slopes typically exhibit extensive, spatially continuous distributions. Their large-scale patterns and relative spatial arrangements provide critical cues for accurate recognition. To meet this need, the OSS auxiliary encoder is designed to model long-range dependencies and extract global geomorphic semantics, effectively compensating for the limited receptive field associated with the CNN-based main encoder.

The encoder adopts a four-stage architecture for multi-scale feature extraction, as illustrated in Fig.4. The first stage consists of a patch embedding layer and an OSS block. The input image X is divided into non-overlapping patches through the patch embedding layer for initial downsampling, after which the OSS block extracts the first-stage features x_1. The second to fourth stages share a unified design, each comprising a patch merging layer and an OSS block. The patch merging layers aggregate adjacent patches, progressively reducing the spatial resolution of the feature maps while enlarging the receptive field and reducing computational complexity. This hierarchical structure enables the encoder to gradually establish a global perspective, allowing it to capture the overall spatial layout and macro-scale morphology of coral reef geomorphology. The OSS blocks in these stages further extract features $x_{2\text{–}4}$ enriched with global contextual information.

The core component of the OSS block is the OSSM, and its architecture is illustrated in Fig.5. The module begins with layer normalization to stabilize the training process. The input is then projected through a linear transformation to adjust its dimensionality, followed by a depthwise convolution to extract spatial features. The OSSM subsequently performs selective scanning along four orientations, resulting in a total of eight scanning directions (Fig.6). The output is passed through another linear transformation and combined with the input features via a residual connection. Through this multi-directional selective scanning mechanism, the OSSM effectively captures the global context of the image. The mechanism allows any element in the feature sequence to interact with elements from all scanning directions, simulating information propagation in multiple directions. This enables the model to capture complex long-range spatial dependencies and obtain a comprehensive representation of global contextual information.

The input and output features of the OSSM are denoted as x_{in} and x_{out}, respectively. The scanning process is described as follows:

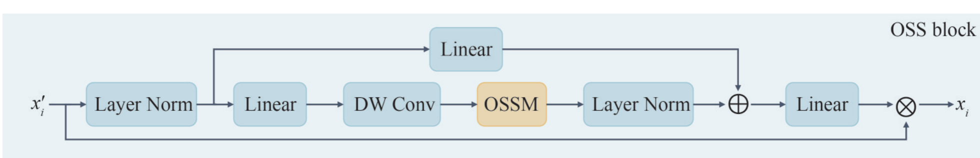

Fig.5 The detailed architecture of Omnidirectional Selective Scanning (OSS) block

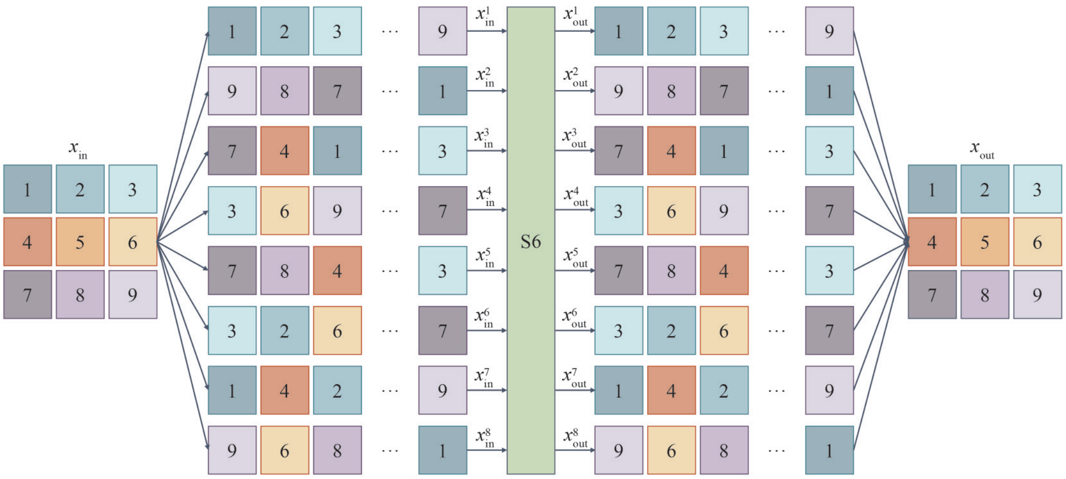

Fig.6 Illustration of the operation of Omnidirectional Selective Scan Module (OSSM)

$$x_{in}^{n} = \mathrm{expand}(x_{in}, n), \quad (1)$$

$$x_{out}^{n} = S6(x_{in}^{n}), \quad (2)$$

$$x_{out} = \mathrm{merge}(x_{out}^{1}, x_{out}^{2}, x_{out}^{3}, x_{out}^{4}, x_{out}^{5}, x_{out}^{6}, x_{out}^{7}, x_{out}^{8}), \quad (3)$$

where $n \in N=\{1, 2, 3, \cdots, 8\}$ denotes the eight scanning directions. The operations expand($\cdot$) and merge($\cdot$) correspond to directional expansion and merging, respectively. $S6(\cdot)$ denotes the selective scanning spatial state sequence model, which enables each pixel in the one-dimensional feature array to interact with previously scanned pixels from other directions by compressing the hidden states. This mechanism establishes a global receptive field (Gu and Dao, 2024) and allows OSSM to aggregate contextual information from the entire image, forming the functional core of its global context modeling capability.

3.2 Main encoder

ResNet18 is employed as the main encoder to capture local information, including subtle textures and spatial patterns on coral reef surfaces. As illustrated in Fig.4, the main encoder comprises four stages corresponding to those of the auxiliary encoder, with each stage containing a residual block and a CCM. The residual blocks perform convolutional operations to extract multi-scale features, denoted as $y_{1\text{–}4}$.

To achieve effective complementarity between global context and local details, features extracted by the auxiliary encoder at each scale are incorporated into the main encoder through the CCM. The CCM employs a parallel dual-branch architecture integrating global and local pathways (Fig.7) and is designed to enable collaborative fusion of features from both encoders. The global branch models long-range dependencies using the local features from the main encoder, while the local branch refines the global features from the auxiliary encoder by enhancing fine-grained details. This design effectively compensates for the limited global perception of the main encoder and the restricted capacity for local modeling of the auxiliary encoder. Such a synergistic mechanism is particularly suitable for coral reef scenes, where large-scale geomorphic patterns coexist with intricate micro-textures, providing essential feature support for distinguishing geomorphic units that share similar local textures but differ in global spatial organization.

The CCM is employed to fuse features from the main encoder, y_i', with features from the auxiliary

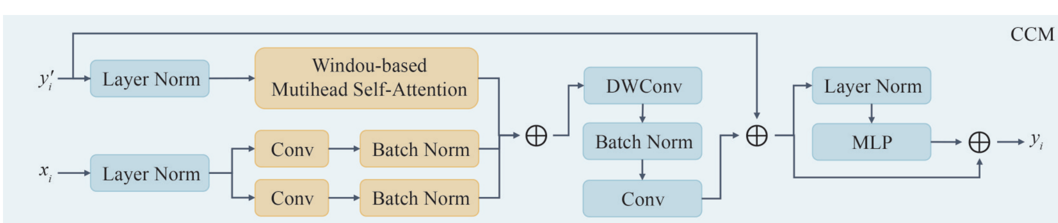

Fig.7 The detailed architecture of Collaborative Completion Module (CCM)

encoder, x_i, where $i \in \{1, 2, 3, 4\}$. In the global branch, the CCM applies window-based multi-head self-attention (WMHSA) to the main encoder features y_i', enabling long-range dependency modeling while maintaining linear computational complexity and enhancing feature representation (Liu et al., 2021). The local branch performs convolutional operations on the auxiliary encoder features x_i, compensating for their emphasis on long-range contextual information and potential limitations in capturing local details. The CCM conducts cross-scale feature fusion at each stage of the main encoder. The fused outputs, y_i, are forwarded to the decoder via skip connections, where the decoder progressively restores spatial resolution and generates the final predictions.

3.3 Decoder

The decoder architecture in this study follows UNetFormer (Wang et al., 2022), and operates in conjunction with the CCM to perform information fusion and fine-grained decision making. It upsamples the multi-scale fused features from the encoder to the original image resolution and generates pixel-level classification maps. As illustrated in Fig.4, the decoder comprises four stages corresponding to those of the encoder.

The first stage incorporates the GLA mechanism, whose architecture is illustrated in Fig.8. Coral reef geomorphology exhibits complex structures and subtle local texture variations in remote sensing imagery, making accurate classification based on local information alone challenging. To address this, GLA is introduced at the decoding stage to jointly model global and local contexts, ensuring that each pixel-level decision integrates both local texture cues and global semantic information. The GLA structure is similar to the CCM in the main encoder but operates on a single input feature.

The input to the first stage is the output feature y_4 from the fourth stage of the main encoder, which is transformed into d_4 by the GLA. The second and third stages consist of a Weighted Sum (WS) operation followed by another GLA. The WS module selectively aggregates the output of the GLA and features from the CCM based on their contribution to segmentation accuracy, thereby learning more generalized fused representations. Its formulation is given by:

$$d_i' = \alpha \cdot y_i + (1 - \alpha) \cdot d_{i+1}, \tag{4}$$

where, feature d_4 passes through the third stage to produce d_3, and is then processed in the second stage to generate d_2. The fourth stage comprises a WS module followed by a Feature Refinement Head (FRH), which further enhances the extracted global-local contextual features and produces the final output d_1. With this hierarchical and lightweight design, the decoder progressively restores spatial details while continuously integrating multi-scale contextual information. This process enables precise delineation of complex coral reef geomorphic boundaries and preserves fine-grained structural details, ultimately achieving high-quality, fine-scale classification.

4 RESULT AND ANALYSIS

4.1 Parameter setting

Experiments were conducted on a single NVIDIA GeForce RTX 3080 Ti GPU with 12 GB of RAM and the PyTorch deep learning framework in Python. For model training, the FCRS-Mamba model was configured with a learning rate (lr) of 0.01 and optimized using the Stochastic Gradient Descent (SGD) optimizer, with a momentum of 0.9 and a weight decay of 0.000 5. The input window size was set to 256×256 pixels with a stride of 32, and the batch size was set to 10. The model was trained for 30 epochs, with performance evaluations conducted at the midpoint and end of each epoch.

In this study, FCRS-Mamba model was comprehensively compared with the RS3Mamba backbone, the high-performance Transformer-based model UNetFormer (Wang et al., 2022), the U-Net-based coral reef geomorphic classification model

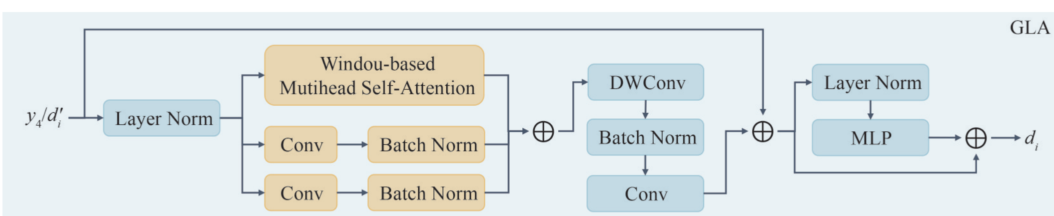

Fig.8 The detailed architecture of Global-Local Attention (GLA)

CU-Net (Zhang et al., 2024), the binary Mamba model VM-Unet (Ruan et al., 2024), and MambaRGBSeg (Li et al., 2024). It is worth noting that MambaRGBSeg was developed from MambaHSI, a model originally designed for hyperspectral remote sensing imagery. To accommodate RGB remote sensing imagery, modules related to hyperspectral feature modeling were removed, while the spatial Mamba blocks were retained and the input structure was redesigned accordingly. To ensure optimal performance for each model, learning rates, optimizers, and scheduler configurations were individually tuned (Table 3), while other parameters were kept consistent with those of FCRS-Mamba. Experiments were conducted under the same computational environment and variable settings to ensure scientific validity and comparability of the results, thereby highlighting the performance advantages of FCRS-Mamba in coral reef geomorphic classification.

Table 3 Training hyperparameter settings for different models

Model	lr	Optimizer	Scheduler
MambaRGBSeg	0.01	Adam	ReduceLROnPlateau
VM-Unet	0.001	Adam	MultiStepLR
CU-Net	0.000 1	Adam	ReduceLROnPlateau
UNetFormer	0.01	SGD	–
RS3Mamba	0.01	SGD	–
FCRS-Mamba	0.01	SGD	–

– means that no learning-rate scheduler was used during model training.

4.2 Evaluation indicator

The performance of the FCRS-Mamba model in coral reef geomorphic classification was evaluated using several metrics, including Overall Accuracy (OA), Kappa coefficient (Kappa), Recall, Mean Recall (mR), F1-score (F1), Mean F1-score (mF1), Intersection over Union (IoU), and Mean IoU (mIoU).

4.3 Results and analysis of geomorphic classification in Antelope Reef

For Sample 3, five rounds of training and testing were conducted for the proposed FCRS-Mamba model and the five comparison models. Table 4 presents the mean Recall for all geomorphic classes across the five runs, along with the mean mR, mF1, mIoU, OA, and Kappa. Since the Antelope Reef test set does not include the five geomorphic classes of

Table 4 Comparison of test results for different models on Antelope Reef (mean±standard deviation of 5 experimental runs, unit: %)

Category	Recall					
	MambaRGBSeg	VM-Unet	CU-Net	UNetFormer	RS3Mamba	FCRS-Mamba
DW	**95.00±0.06**	91.43±0.13	96.24±0.15	92.12±0.09	82.77±0.07	87.17±0.05
DFS	80.68±0.17	**85.72±0.12**	81.73±0.18	76.55±0.37	80.16±0.16	77.65±0.35
SFS	84.98±0.06	86.52±0.17	76.87±0.25	84.12±0.11	84.71±0.04	**87.04±0.01**
RC	83.06±0.40	81.13±0.30	**84.16±0.54**	80.25±0.12	81.84±0.01	81.68±0.08
AR	86.53±0.39	90.81±0.10	93.16±0.08	94.58±0.04	95.78±0.01	**95.98±0.02**
RA	84.54±0.03	88.37±0.02	86.67±0.04	82.36±0.67	**88.45±0.02**	87.98±0.03
DCA	76.20±3.18	70.74±0.26	89.91±0.30	92.72±0.07	92.00±0.15	**95.26±0.08**
SCA	91.91±0.03	86.03±0.47	93.66±0.12	94.23±0.05	**95.47±0.00**	92.71±0.03
L	73.46±4.44	86.91±0.23	92.58±0.20	96.87±0.00	97.23±0.01	**98.35±0.01**
LPPR	48.03±2.75	46.56±6.66	66.56±1.90	**94.15±0.01**	93.21±0.05	90.84±0.05
mR	80.44±0.01	81.42±0.04	86.15±0.02	88.79±0.00	89.16±0.00	**89.46±0.00**
mF1	78.40±0.03	79.99±0.06	85.65±0.03	88.21±0.01	89.18±0.00	**89.56±0.00**
mIoU	66.46±0.05	68.74±0.04	75.83±0.05	79.40±0.02	80.82±0.00	**81.49±0.00**
OA	81.30±0.17	84.65±0.02	88.95±0.01	90.29±0.01	91.16±0.00	**91.67±0.00**
Kappa	78.40±0.20	82.04±0.02	86.99±0.01	88.56±0.01	89.63±0.00	**90.16±0.00**
Max_mIoU	69.17	71.98	78.72	80.86	81.16	**81.85**

Bold indicates the best result achieved among different models under the same geomorphic category or evaluation metric.

LFPR, B, S, MSA, and V, the accuracy analysis was performed only on the ten geomorphic classes present in the test set.

The experimental results presented in Table 4 demonstrate the superior performance of the FCRS-Mamba model in coral reef geomorphic classification, with comprehensive evaluation metrics significantly exceeding those of the comparison models. Specifically, the model achieved outstanding results of 91.67% and 81.49% in OA and mIoU, respectively, with a Max_mIoU of 81.85%. Compared with the original RS3Mamba model, FCRS-Mamba improved Recall for approximately half of the key geomorphic categories, including DW and AR, resulting in a 0.67% increase in mIoU. This confirms the effectiveness of the structural enhancements in improving feature discrimination. In lateral comparisons, the advantages of FCRS-Mamba are even more pronounced. Its mIoU exceeds those of MambaRGBSeg (66.46%), VM-Unet (68.74%), CU-Net (75.83%), and UNetFormer (79.40%) by 15.03, 12.75, 5.66, and 2.09 percentage points, respectively, with OA showing similar gains. Notably, for small-scale and challenging geomorphic categories such as LPPR, FCRS-Mamba demonstrated markedly superior precision in feature capture compared with the other models. This provides strong evidence of its enhanced ability to resolve fine-scale details in complex scenarios characterized by high intra-category variability and inter-category similarity, ultimately ensuring higher classification consistency and reduced misclassification across the entire study area.

FCRS-Mamba not only achieves leading mean metrics but also maintains a standard deviation of 0, which is significantly lower than those of all other models except RS3Mamba. This demonstrates stability and reliability across repeated experiments. Such consistency allows FCRS-Mamba to produce high-precision results reliably, minimizing performance fluctuations and reducing uncertainty in practical applications, thereby providing a robust technical foundation for coral reef geomorphic category classification.

A comparison of the test results of FCRS-Mamba and RS3Mamba in Fig.9 shows that in Samples 1–5, RS3Mamba misclassified DCA as SCA, and in Samples 1–9, it incorrectly labeled the L as LFPR. Although RS3Mamba performed slightly better in Samples 1–13, consistent with the higher Recall observed for DCA in Table 4, the overall classification results of FCRS-Mamba showed closer agreement with the ground truth labels. Lateral comparisons with other models further highlight the advantages of FCRS-Mamba. In Samples 1–5 and 1–9, FCRS-Mamba demonstrated notable superiority. Specifically, in Samples 1–5, it avoided the common misclassification of DCA observed in most models and identified the RA more accurately than UNetFormer. Similarly, in Samples 1–9, its delineation accuracy remained outstanding. While VM-Unet achieved results close to the ground truth in Samples 1–13, its performance in other

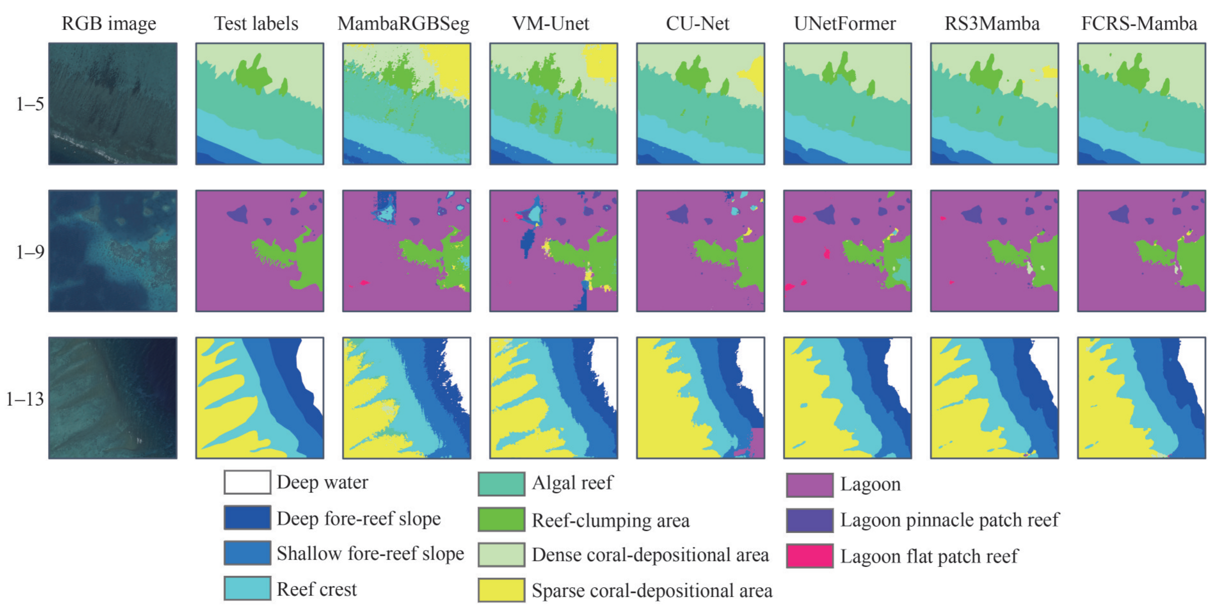

Fig.9 Classification results of test set from Antelope Reef

samples was inferior. Overall, these analyses indicate that FCRS-Mamba maintains consistently superior performance across multiple samples, showing clear advantages in both complex geomorphic category recognition and generalization capability, thereby confirming its comprehensive superiority in coral reef geomorphic classification tasks.

Based on the models trained to achieve optimal mIoU, a full-scale geomorphic classification of Antelope Reef was conducted, with the reef area masked accordingly. The classification results are shown in Fig.10. Among all methods, FCRS-Mamba (Fig.10a) produced the most accurate classification of geomorphic categories on Antelope Reef, while the results of the five comparison models are presented in Fig.10b–f. Among these models, RS3Mamba performed the best, yielding results most similar to those of FCRS-Mamba, although notable misclassifications remained, particularly in the complex geomorphic region of the northwest portion of the reef. UNetFormer and CU-Net showed comparable performance, both exhibiting substantial class confusion. Specifically, the boundaries between the L and DCA were blurred, and RC was frequently misclassified as DCA, with CU-Net performing worse. Both models also struggled to distinguish between DFS and SFS. VM-Unet, due to its per-pixel classification mechanism without spatial context integration, produced highly fragmented classification maps and the lowest overall classification quality. MambaRGBSeg demonstrated relatively good recognition of L but performed poorly in identifying other geomorphic categories. This model nearly failed to detect LPPR and LFPR, frequently confused DCA with SCA, misclassified AR as

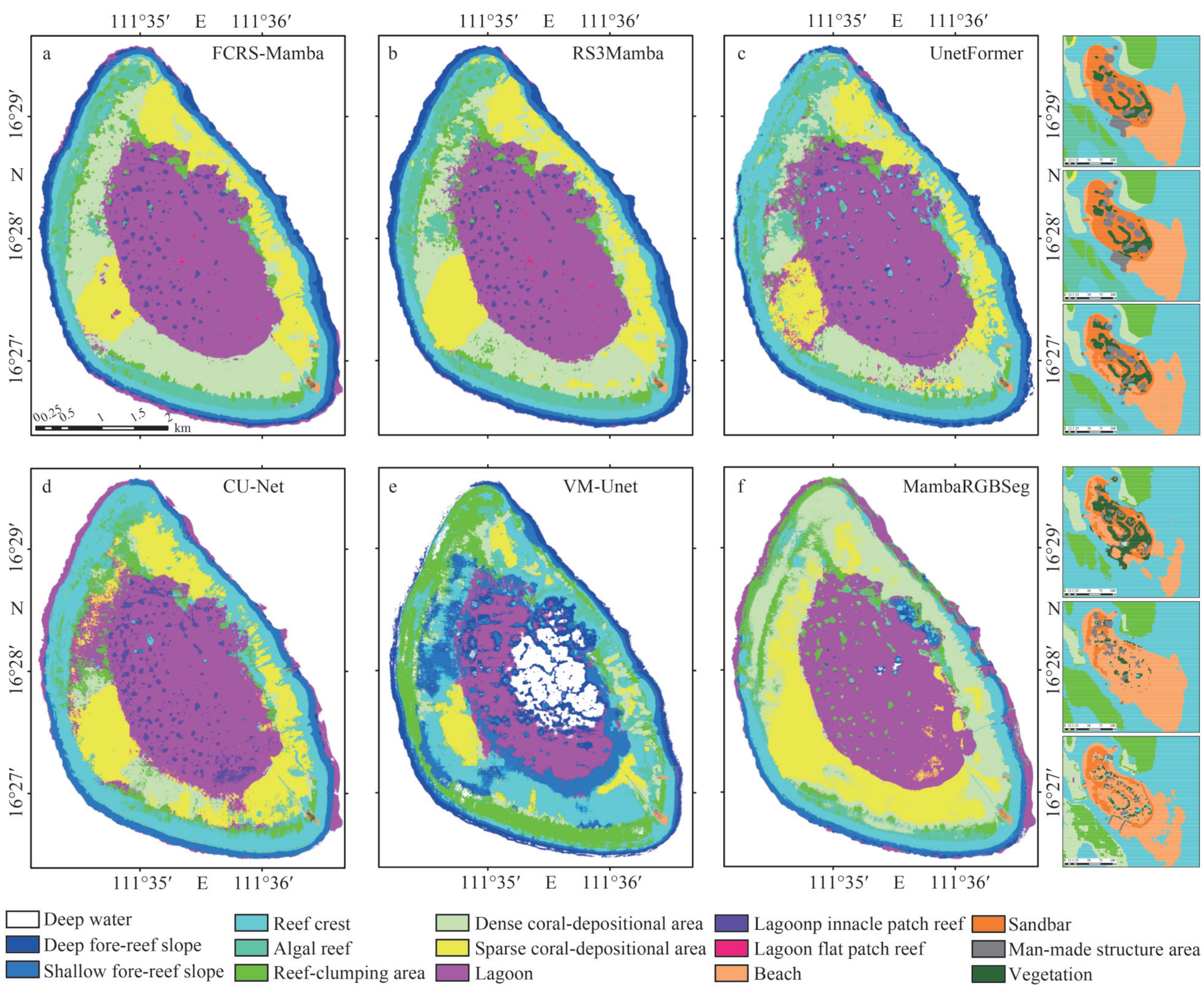

Fig.10 Coral reef geomorphic classification results of different models on Antelope Reef

The local insets on the right, showing the Kuangzai sand cay, correspond from top to bottom and left to right to the respective full-scene classification maps of Antelope Reef.

DCA, and showed extensive misclassification between RC and RA.

A comprehensive comparison of the classification results across all models demonstrates that the FCRS-Mamba delivers outstanding performance in coral reef geomorphic classification. Compared with the other models, FCRS-Mamba more accurately identifies and differentiates geomorphic categories, effectively avoiding severe misclassifications and class confusion. As a result, the model achieves substantially improved classification accuracy and reliability, providing a robust technical foundation for research on coral reef geomorphology.

5 DISCUSSION

5.1 The impact of the number of feature search directions on classification performance

Compared with RS3Mamba, FCRS-Mamba expands the selective scanning strategy from four directions to eight, and the associated quantitative improvements have been examined earlier. In this section, a detailed visual comparison of the classification results of FCRS-Mamba and RS3Mamba is presented based on Fig.10a and b. As illustrated in Fig.11, this comparison clearly demonstrates the substantial advantages of the improved model in complex geomorphic regions.

In the northwestern portion of Antelope Reef, where the geomorphic classes are most complex, the FCRS-Mamba model delineates the boundary of the L with markedly higher precision (Fig.11a). In contrast, RS3Mamba shows a clear overflow along the L edges (Fig.11d), which leads to blurred and overlapping boundaries between the L and the DCA, thereby weakening the distinction between these geomorphic categories. RS3Mamba also exhibits a higher tendency to misclassify DCA as AR, producing fragmented and visually disorderly classification patterns in this region. By comparison, the outputs generated by FCRS-Mamba (Fig.10a) present sharper boundaries and more coherent spatial organization of geomorphic categories.

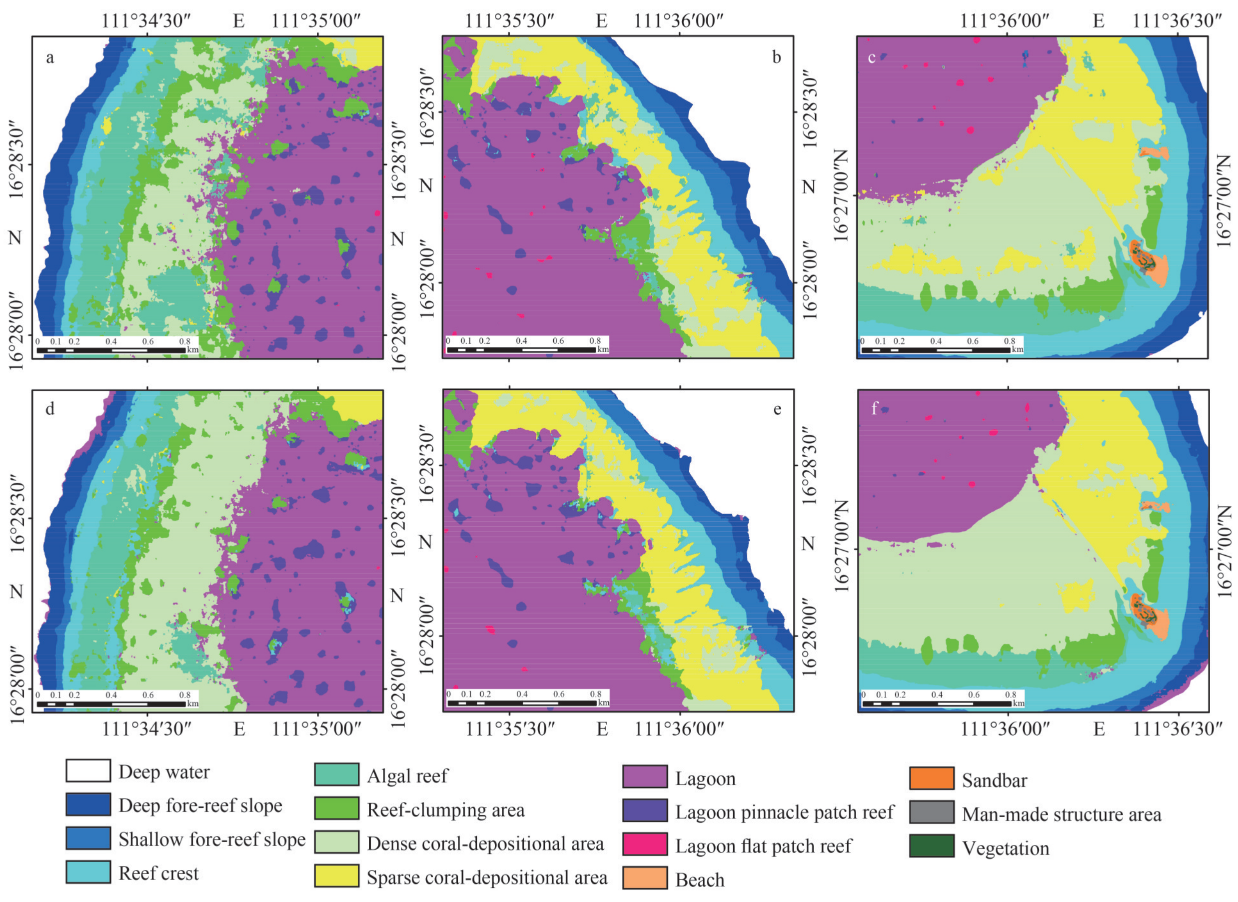

Fig.11 Local coral reef geomorphic classification results of FCRS-Mamba and RS3Mamba on Antelope Reef

a–c. local coral reef geomorphic classification results of RS3Mamba on Antelope Reef, corresponding to Fig.10b; d–f. local coral reef geomorphic classification results of FCRS-Mamba on Antelope Reef, corresponding to Fig.10a.

Further examination of Fig.11b–c and Fig.11e–f indicates that the expanded scanning strategy of FCRS-Mamba, which increases the scanning directions from four to eight, markedly enhances its adaptability in complex geomorphic regions. This modification reduces misclassifications and class confusion and results in clearer geomorphic boundaries and more accurate spatial distribution patterns across distinct geomorphic categories.

Although the proposed eight-direction selective scanning strategy introduces additional computational overhead compared with the conventional four-direction scanning scheme, the increase remains limited. Under the same experimental environment, the average training time of RS3Mamba was approximately 3.25 h, whereas FCRS-Mamba required approximately 3.63 h, corresponding to an increase of only 0.38 h (11.69%). Considering the significant improvements achieved by FCRS-Mamba in both classification accuracy and geomorphic boundary delineation, this additional computational overhead is reasonable and acceptable, indicating that the proposed model achieves a favorable balance between computational efficiency and classification performance.

5.2 The impact of sample selection strategy on classification performance

In RGB satellite imagery, the lagoonal deep-water zone is highly vulnerable to misclassification as open-ocean deep water because the two show nearly indistinguishable pixel reflectance patterns (Fig.12a).

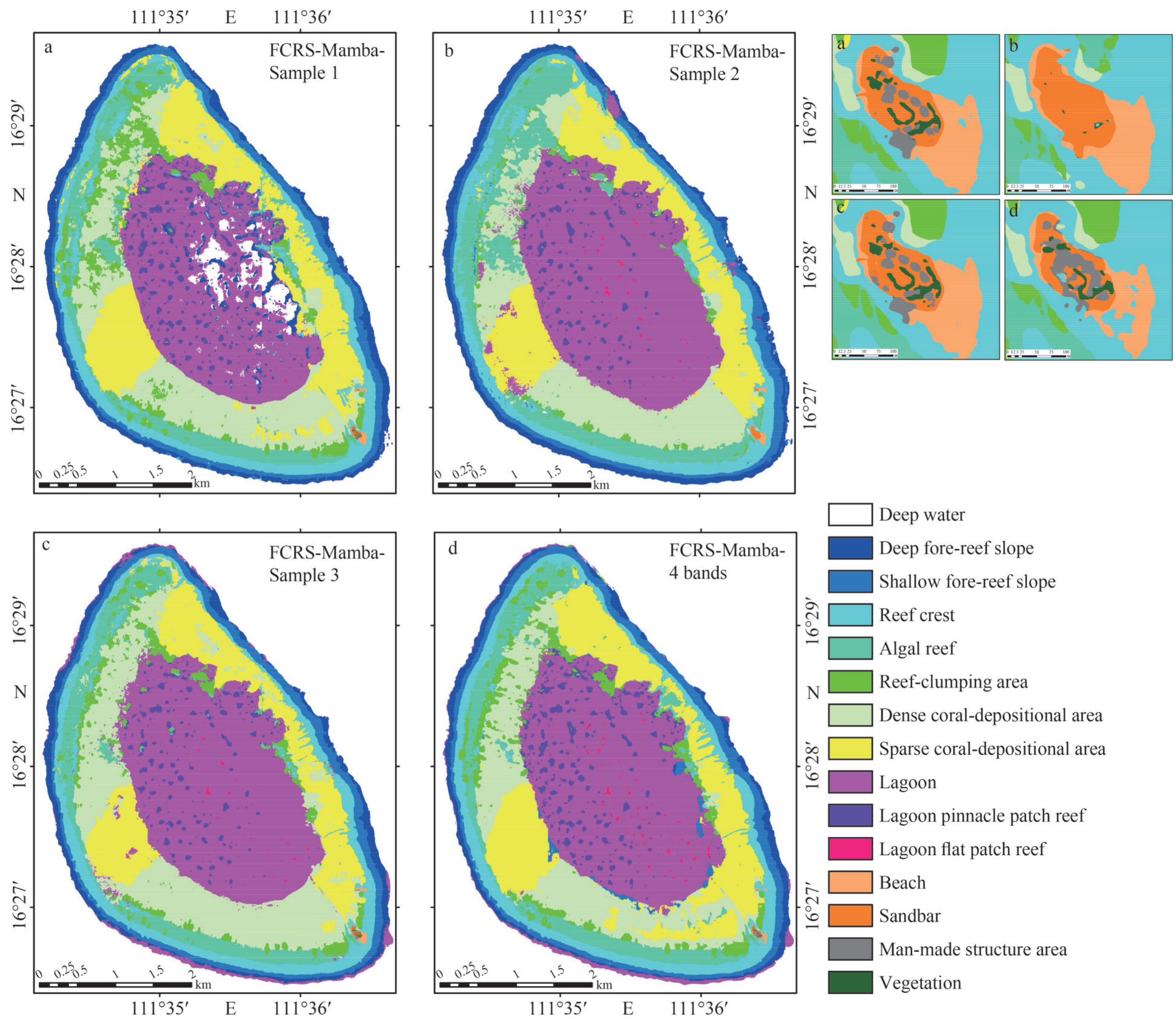

Fig.12 Coral reef geomorphic classification results under different experimental settings on Antelope Reef

The local enlarged insets of the Kuangzai sand cay shown in the upper-right corner correspond to the full-scene classification maps of Antelope Reef in the same order.

Based on the visualized classification results in Fig.12 and the quantitative evaluation metrics in Table 5, this study provides a systematic assessment of the three sample-selection strategies introduced in Section 2.3 for geomorphic classification of Antelope Reef.

The experimental results indicate that although the discrete-sample setting (Sample 1) achieves relatively high accuracy (mR=89.87%, mF1=89.15%, mIoU=80.85%) and even exceeds Sample 3 in terms of mR (89.46%), it still produces substantial misclassification of the lagoonal deep-water zone during full-scene geomorphic classification of Antelope Reef, where these pixels are frequently confused with DW or DFS (Fig.12a). The cross-reef sample setting (Sample 2) effectively avoids this misclassification issue (Fig.12b), yet its overall accuracy remains unsatisfactory, with its mIoU being 2.59% lower than that of Sample 3, making it the least accurate among the three strategies. Sample 3, designed as an improved scheme, achieves more reliable classification results (Fig.12c, consistent with Fig.10a). Except for the mR metric, the accuracy ranking of the three settings follows the order Sample 3>Sample 1>Sample 2. A visual comparison of Fig.12a–c further shows that the mixed-sample strategy in Sample 3 not only yields the highest accuracy but also eliminates the misclassification of lagoonal deep-water pixels. These findings confirm that Sample 3 represents the most effective sampling strategy for geomorphic classification of Antelope Reef.

5.3 Experiment and analysis of model generalization capability

To comprehensively evaluate the applicability and robustness of model across different datasets and geographic settings, an additional geomorphic classification experiment was carried out in the North Reef region. Both quantitative metrics and visual assessment were employed to systematically compare the performance of FCRS-Mamba with the other methods (Table 6 and Fig.13).

The experimental results show that FCRS-Mamba performs strongly across multiple evaluation metrics (Table 6). The OA and Kappa reach 93.57% and 91.58%, respectively, and except for a standard deviation of 0.01% in mR, all other metrics record zero standard deviation, indicating high stability of the method. For small-scale geomorphic categories, the model demonstrates particularly strong capability in identifying LPPR and LFPR, with Recall values of 78.42% and 78.45%, respectively, both of which are markedly higher than those of the comparison models. The visualized classification results (Fig.13) further illustrate that FCRS-Mamba detects a greater number of SFS and patch reef features while substantially reducing confusion with the L. Although a misclassification occurs for the DCA on the left side due to the presence of only one test sample, the model maintains clear advantages across all remaining geomorphic categories. The findings in the North Reef region are consistent with the earlier results for Antelope Reef, jointly

Table 5 Comparison of test results under different sampling strategies on Antelope Reef (mean of 5 experimental runs, unit: %)

Category	Recall			F1			IoU		
	S1	S2	S3	S1	S2	S3	S1	S2	S3
DW	88.08	**96.83**	87.17	92.22	**96.41**	91.20	85.66	**93.10**	83.87
DFS	81.43	**89.18**	77.65	**84.60**	84.41	82.29	**73.38**	73.06	70.08
SFS	**87.87**	86.08	87.04	87.36	**89.10**	85.92	77.57	**80.36**	75.35
RC	84.81	**87.51**	81.68	**85.92**	80.89	84.49	**75.36**	68.04	73.17
AR	95.12	69.13	**95.98**	**94.50**	76.04	94.43	**89.59**	61.47	89.46
RA	**88.19**	87.06	87.98	89.73	82.60	**90.04**	81.38	70.41	**81.92**
DCA	**95.35**	91.74	95.26	92.24	92.41	**94.52**	85.66	85.94	**89.65**
SCA	91.26	**93.74**	92.71	87.51	**95.05**	87.97	77.84	**90.57**	78.60
L	95.48	98.06	**98.35**	97.31	97.33	**98.38**	94.76	94.80	**96.81**
LPPR	**91.11**	79.99	90.84	80.13	83.15	**86.37**	67.29	71.29	**76.04**
Mean	**89.87**	87.93	89.46	89.15	87.74	**89.56**	80.85	78.90	**81.49**

Bold indicates the best result achieved among different sampling strategies under the same geomorphic category or evaluation metric.

Table 6 Comparison of test results for different models on North Reef (mean±standard deviation of 5 experimental runs, unit: %)

Category	Recall					
	MambaRGBSeg	VM-Unet	CU-Net	UNetFormer	RS3Mamba	FCRS-Mamba
DW	98.70±0.01	99.36±0.01	99.52±0.00	99.90±0.00	99.55±0.01	**99.95±0.00**
SFS	87.17±0.58	95.16±0.02	95.85±0.02	**96.40±0.01**	96.17±0.01	96.36±0.00
RC	86.84±0.43	95.16±0.01	**96.51±0.04**	93.73±0.03	96.24±0.00	96.05±0.01
RA	87.86±0.16	85.15±0.20	**90.38±0.03**	87.93±0.01	89.44±0.00	89.07±0.00
DCA	96.38±0.02	97.28±0.00	96.54±0.03	**98.46±0.00**	98.14±0.00	98.43±0.00
L	65.40±1.60	64.73±0.87	74.84±1.25	89.33±0.06	**91.29±0.05**	90.37±0.01
LPPR	7.74±1.99	31.14±10.37	8.73±0.58	67.01±1.93	73.13±0.69	**78.42±0.20**
LFPR	0.43±0.01	57.12±6.25	60.26±1.79	75.68±0.09	70.21±1.11	**78.45±0.28**
mR	66.32±0.02	78.01±0.07	77.83±0.03	88.56±0.03	89.27±0.02	**90.89±0.01**
mF1	62.09±0.02	70.73±0.01	75.54±0.02	84.87±0.01	84.94±0.01	**85.60±0.00**
mIoU	53.49±0.04	60.04±0.01	65.71±0.03	76.31±0.01	76.84±0.01	**77.43±0.00**
OA	83.42±0.10	85.36±0.01	88.83±0.06	92.85±0.00	**93.57±0.00**	**93.57±0.00**
Kappa	78.51±0.16	81.08±0.02	85.53±0.09	90.62±0.01	**91.58±0.00**	**91.58±0.00**
Max_mIoU	55.83	61.30	68.66	77.78	78.08	78.42

Bold indicates the best result achieved among different models under the same geomorphic category or evaluation metric.

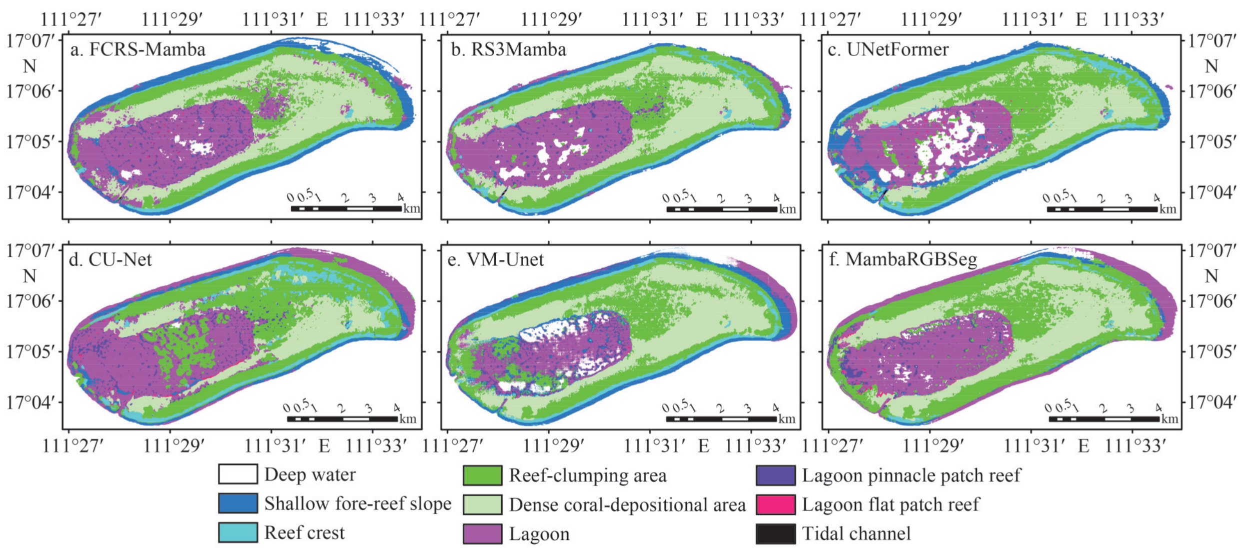

Fig.13 Coral reef geomorphic classification results of different models on North Reef

confirming that FCRS-Mamba exhibits strong applicability and reliability in different environments.

A comparative analysis of Tables 4 and 6 shows that, despite covering a greater variety of geomorphic categories, Antelope Reef classified using 0.5-m high-resolution BJ-3A imagery outperforms North Reef mapped with 4 m resolution GF-2 imagery, with mF1 and mIoU increased by 3.96% and 4.06%, respectively. The advantage of high-resolution imagery is particularly evident for small-scale geomorphic categories such as LPPR, where the Recall for Antelope Reef improves by 12.42% compared with North Reef. These results clearly indicate that higher spatial resolution imagery effectively enhances the identification of fine-scale coral reef geomorphic categories, thereby substantially improving overall classification accuracy.

5.4 The impact of near-infrared bands on classification performance

In the infrared bands, water absorbs substantially more energy than in the visible bands. Even in very shallow areas, water absorbs nearly all incident energy in the near-infrared (NIR) and mid-infrared wavelengths, resulting in minimal reflected energy (Chen et al., 2022). This feature is clearly illustrated in Fig.14a–d. Compared with other spectral bands, the NIR image (770–890 nm; Fig.14d) contains limited useful information, with strong reflectance observed only over exposed features such as Kuangzai Sandbar and adjacent low-tide reef terraces.

This study assessed the contribution of the NIR band to coral reef geomorphic classification. Table 7 presents classification results for Antelope Reef using four bands (blue, green, red, and NIR) and three bands (blue, green, red). For DFS, RC, and SCA, the 4-band dataset achieves IoU values that are 3.73%, 1.90%, and 0.43% higher than those of the 3-band dataset, which aligns with the information patterns observed in Fig.14d. This suggests that the NIR band helps distinguish these specific geomorphic categories. However, considering overall classification performance, the 3-band data achieve higher accuracy across a broader range of geomorphic categories. In particular, the IoU for DCA is 4.62% higher, and the mean values of the three evaluation metrics exceed those of the 4-band data by 0.19%, 0.36%, and 0.70%, respectively. These findings indicate that although the NIR band provides some benefits for certain categories, its strong absorption by water limits the available information, which can interfere with accurate classification of other geomorphic categories. Consequently, the 4-band dataset exhibits lower

Table 7 Comparison of test results between 3-band and 4-band data for Antelope Reef (mean of 5 experimental results, unit: %)

Category	Recall		F1		IoU	
	4-band	3-band	4-band	3-band	4-band	3-band
DW	84.62	**87.17**	89.52	**91.20**	81.09	**83.87**
DFS	**83.88**	77.65	**84.90**	82.29	**73.81**	70.08
SFS	84.37	**87.04**	85.90	**85.92**	75.30	**75.35**
RC	**83.99**	81.68	**85.74**	84.49	**75.07**	73.17
AR	94.16	**95.98**	94.38	**94.43**	89.36	**89.46**
RA	85.57	**87.98**	89.31	**90.04**	80.69	**81.92**
DCA	92.36	**95.26**	91.84	**94.52**	85.03	**89.65**
SCA	**94.84**	92.71	**88.27**	87.97	**79.03**	78.60
L	97.27	**98.35**	97.68	**98.38**	95.47	**96.81**
LPPR	**91.62**	90.84	84.44	**86.37**	73.11	**76.04**
Mean	89.27	**89.46**	89.20	**89.56**	80.79	**81.49**

Bold indicates the best result achieved among different band data under the same geomorphic category or evaluation metric.

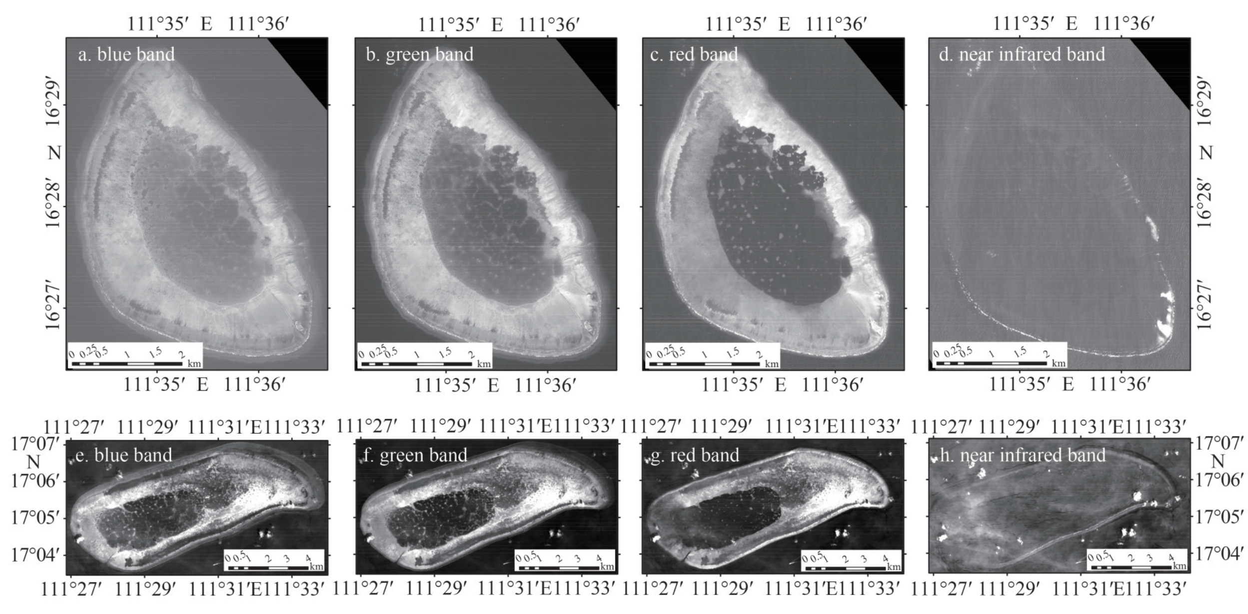

Fig.14 Multispectral band images of Antelope Reef and North Reef

a. Antelope Reef, blue band: 450–520 nm; b. Antelope Reef, green band: 520–590 nm; c. Antelope Reef, red band: 630–690 nm; d. Antelope Reef, NIR band: 770–890 nm; e. North Reef, blue band: 450–520 nm; f. North Reef, green band: 520–590 nm; g. North Reef, red band: 630–690 nm; h. North Reef, NIR band: 770–890 nm.

overall classification accuracy than the 3-band dataset.

This study compared classification results obtained from the 4-band dataset (Fig.12d) and the 3-band dataset (Fig.12c). While the overall geomorphic patterns are similar, notable differences appear at the local scale. For instance, in the SCA area at the southwestern corner of Antelope Reef, the 4-band dataset benefits from spectral information provided by the NIR band, reducing misclassification of scattered L pixels within the SCA. However, along the edges of the L, some pixels are incorrectly assigned to DFS and SFS. In the Kuangzai Sandbar, the 3-band dataset demonstrates superior classification accuracy, precisely delineating the boundaries and morphology of the MSA and more accurately distinguishing the B geomorphic category. Meanwhile, in the DCA region west of Kuangzai Sandbar, the 4-band dataset misclassifies DCA pixels as SCA. A comprehensive comparison of qualitative observations and quantitative metrics indicates that inclusion of the NIR band in the 4-band dataset introduces misclassifications and redundant information, which negatively affects overall performance. These findings further confirm that the 3-band dataset provides higher applicability and classification accuracy for geomorphic classification of Antelope Reef.

To further evaluate the generality of the limited reflectance characteristic of the NIR band, a comparative experiment was conducted in the North Reef. Comparison of the NIR image (Fig.14h) with the other three spectral bands (Fig.14e–g) indicates that the NIR band similarly contains sparse useful information in North Reef. Moreover, in regions affected by clouds and haze, the NIR band exhibits high reflectance, providing little effective information for geomorphic classification.

In the North Reef, this study also compared evaluation metrics for each geomorphic category in the test set using 4-band and 3-band datasets (Table 8), along with their corresponding visual classification results (Fig.15). As shown in Table 8, the 3-band dataset not only achieves clear advantages for key geomorphic categories such as LPPR and LFPR, but also exhibits higher mean values across all evaluation metrics compared with the 4-band dataset. The visual classification results

Table 8 Comparison of test results between 3-band and 4-band data for North Reef (mean of 5 experimental results, unit: %)

Category	Recall		F1		IoU	
	4-band	3-band	4-band	3-band	4-band	3-band
DW	99.79	**99.95**	**93.85**	93.41	**88.43**	87.64
SFS	**96.67**	96.36	96.82	**97.04**	93.85	**94.25**
RC	**96.11**	96.05	**90.63**	89.11	**82.88**	80.38
RA	**89.83**	89.07	**93.61**	93.22	**87.99**	87.31
DCA	**98.53**	98.43	93.91	**95.40**	88.56	**91.21**
L	87.44	**90.37**	92.12	**94.17**	85.46	**88.99**
LPPR	64.19	**78.42**	51.12	**52.17**	34.46	**35.37**
LFPR	67.40	**78.45**	69.28	**70.28**	53.17	**54.28**
Mean	87.50	**90.89**	85.17	**85.60**	76.85	**77.43**

Bold indicates the best result achieved among different band data under the same geomorphic category or evaluation metric.

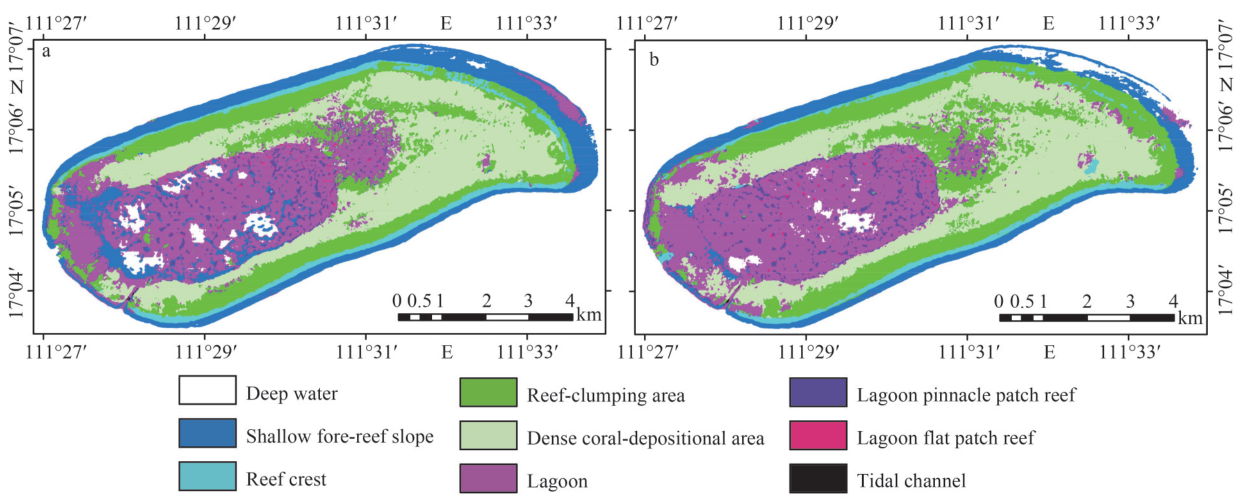

Fig.15 Geomorphic classification results using 4-band and 3-band data on North Reef

a. classification result using the 4-band data; b. classification result using the 3-band data.

(Fig.15) indicate that the 4-band dataset fails to resolve misclassification issues between DCA and L, as well as between RA and L. In fact, it exacerbates these errors and introduces additional misclassifications in DW areas and SFS regions. Although the 4-band dataset shows slight improvements in a few geomorphic categories, such as DW and RC, and displays some advantage in SFS recognition, these localized improvements do not compensate for its overall negative impact. Furthermore, under cloud and haze interference, the IoU for DCA decreases by 2.65%, providing additional evidence that inclusion of the NIR band can reduce overall classification accuracy.

In summary, the application of the NIR band in coral reef geomorphic classification is constrained by both water and cloud or haze effects. Strong absorption of NIR energy by water produces dark regions in imagery, which not only obscure underwater geomorphic details but also increase the likelihood of confusion with other low-reflectance surfaces. Meanwhile, water droplets and ice crystals in clouds and haze induce absorption and scattering of NIR radiation, disturbing energy distribution, reducing image contrast and feature clarity, and potentially generating spurious reflectance signals. These factors can further interfere with atmospheric correction, degrading data quality and ultimately reducing classification reliability and accuracy. Consequently, although the NIR band may provide some geomorphic information, its effectiveness is outweighed by these negative effects. Developing methods to mitigate such interferences and fully exploit the potential of the NIR band for coral reef geomorphic classification represents an important direction for future research.

6 CONCLUSION

This study conducted an innovative investigation into coral reef geomorphic classification, achieving significant progress in three aspects, namely model development, model comparison, and spectral band analysis. First, to address the challenges posed by complex and multi-scale geomorphic features in coral reef remote sensing imagery and the limitations of conventional model search strategies, the proposed FCRS-Mamba framework optimizes the VSS block in RS3Mamba by expanding its four-directional scanning to an eight-directional OSS block. This enhancement substantially improves the ability to extract multi-directional spatial features from high-resolution imagery. Experimental results show that FCRS-Mamba achieves excellent performance in both Antelope Reef and North Reef, with mIoU values of 81.49% and 77.43%, respectively, corresponding to improvements of 0.67%–15.03% and 0.59%–23.94% over other methods based on Mamba, CNN, or Transformer architectures. Second, the application of coral reef remote sensing data was systematically investigated by comparing RGB three-band datasets with four-band datasets that include the NIR band. The results indicate that inclusion of the NIR band can negatively affect classification accuracy, whereas RGB imagery alone provides satisfactory performance. This finding expands potential sources of coral reef data and facilitates broader application of FCRS-Mamba in geomorphic classification tasks. Overall, this study lays the foundation for large-scale, high-precision coral reef geomorphic classification and provides strong technical support for coral reef ecological monitoring and conservation.

7 DATA AVAILABILITY STATEMENT

Data are available on request due to privacy or other restrictions.

8 ACKNOWLEDGMENT

The authors gratefully acknowledge the South China Sea Institute of Oceanology, Chinese Academy of Sciences, for providing field survey data, and Shandong Twenty First Century Aerospace Information Technology Co., Ltd. for supplying the Beijing-3A satellite imagery of Antelope Reef.

References

Ai B, Liu X, Wen Z et al. 2024. A novel coral reef classification method combining radiative transfer model with deep learning. *IEEE Journal of Selected Topics in Applied Earth Observations and Remote Sensing*, **17**: 13400-13412, https://doi.org/10.1109/JSTARS.2024.3430899.

Bajjouk T, Mouquet P, Ropert M et al. 2019. Detection of changes in shallow coral reefs status: towards a spatial approach using hyperspectral and multispectral data. *Ecological Indicators*, **96**: 174-191, https://doi.org/10.1016/j.ecolind.2018.08.052.

Chan Y K S, Ng C S L, Tun K P P et al. 2024. Decadal decline of functional diversity despite increasing taxonomic and phylogenetic diversity of coral reefs under chronic urbanisation stress. *Ecological Indicators*, **164**: 112143, https://doi.org/10.1016/j.ecolind.2024.112143.

Chen K Y, Chen B W, Liu C Y et al. 2024. RSMamba:

remote sensing image classification with state space model. *IEEE Geoscience and Remote Sensing Letters*, **21**: 8002605, https://doi.org/10.1109/LGRS.2024.3407111.

Chen L F, Lee Z P, Lin G et al. 2022. Experimental evaluation of temperature dependence of pure water absorption coefficient in near-infrared domain. *Acta Optica Sinica*, **42**(18): 1801007, https://doi.org/10.3788/AOS202242.1801007. (in Chinese with English abstract)

Dang K B, Nguyen T H T, Nguyen H D et al. 2022. U-shaped deep-learning models for island ecosystem type classification, a case study in Con Dao Island of Vietnam. *One Ecosystem*, **7**: e79160, https://doi.org/10.3897/oneeco.7.e79160.

Dong J. 2021. Estimation and analysis of living coral cover in Xisha Islands based on high resolution satellite remote sensing. First Institute of Oceanography, Ministry of Natural Resources, Qingdao. (in Chinese with English abstract)

Gapper J J, El-Askary H, Linstead E et al. 2019. Coral reef change detection in remote Pacific islands using support vector machine classifiers. *Remote Sensing*, **11**(13): 1525, https://doi.org/10.3390/rs11131525.

Giles A B, Ren K, Davies J E et al. 2023. Combining drones and deep learning to automate coral reef assessment with RGB imagery. *Remote Sensing*, **15**(9): 2238, https://doi.org/10.3390/rs15092238.

Gong J M, Zhu G Q, Yang J et al. 2014. A study on the object-oriented model for geomorphic unit extraction of coral reefs in the South China Sea. *Journal of Geo-Information Science*, **16**(6): 997-1004, https://doi.org/10.3724/SP.J.1047.2014.00997. (in Chinese with English abstract)

Gu A, Dao T. 2024. Mamba: linear-time sequence modeling with selective state spaces. arXiv preprint arXiv:2312.00752, https://doi.org/10.48550/arXiv.2312.00752.

Gu A, Goel K, Ré C. 2022. Efficiently modeling long sequences with structured state spaces. arXiv preprint arXiv:2111.00396, https://doi.org/10.48550/arXiv.2111.00396.

He X H, Cao K, Yan K Y et al. 2024. Pan-Mamba: effective pan-sharpening with state space model. arXiv preprint arXiv:2402.12192, https://doi.org/10.48550/arXiv.2402.12192.

Hedley J D, Roelfsema C, Brando V et al. 2018. Coral reef applications of Sentinel-2: coverage, characteristics, bathymetry and benthic mapping with comparison to Landsat 8. *Remote Sensing of Environment*, **216**: 598-614, https://doi.org/10.1016/j.rse.2018.07.014.

Hochberg E J, Atkinson M J. 2003. Capabilities of remote sensors to classify coral, algae, and sand as pure and mixed spectra. *Remote Sensing of Environment*, **85**(2): 174-189, https://doi.org/10.1016/S0034-4257(02)00202-X.

Hu L Q, Liu Y L, Ren Y H et al. 2010. Research on the extraction method of coral reef at Spratly Islands using SPOT5. *Remote Sensing Technology and Application*, **25**(4): 493-501, https://doi.org/10.11873/j.issn.1004-0323.2010.4.493. (in Chinese with English abstract)

Hu Y, Ma X P, Sui J L et al. 2024. PPMamba: a pyramid pooling local auxiliary SSM-based model for remote sensing image semantic segmentation. arXiv preprint arXiv:2409.06309, https://doi.org/10.48550/arXiv.2409.06309.

Ji X, Yang B S, Wei Z et al. 2024. Benthic habitat sediments mapping in coral reef area using amalgamation of multi-source and multi-modal remote sensing data. *Remote Sensing of Environment*, **304**: 114032, https://doi.org/10.1016/j.rse.2024.114032.

King A, Bhandarkar S M, Hopkinson B M. 2018. A comparison of deep learning methods for semantic segmentation of coral reef survey images. *In*: 2018 IEEE/CVF Conference on Computer Vision and Pattern Recognition Workshops (CVPRW). IEEE, Salt Lake City, UT, USA. p.1475-1483, https://doi.org/10.1109/CVPRW.2018.00188.

Li J W, Knapp D E, Fabina N S et al. 2020. A global coral reef probability map generated using convolutional neural networks. *Coral Reefs*, **39**(6): 1805-1815, https://doi.org/10.1007/s00338-020-02005-6.

Li T C, Feng J L, Zhao L et al. 2024a. Geographical distribution of coral reefs and their responses to environmental factors in the South China Sea. *Ecological Indicators*, **158**: 111485, https://doi.org/10.1016/j.ecolind.2023.111485.

Li Y P, Luo Y, Zhang L F et al. 2024b. MambaHSI: spatial-spectral mamba for hyperspectral image classification. *IEEE Transactions on Geoscience and Remote Sensing*, **62**: 5524216, https://doi.org/10.1109/TGRS.2024.3430985.

Liu Y, Tian Y J, Zhao Y Z et al. 2024. VMamba: visual state space model. arXiv preprint arXiv:2401.10166, https://doi.org/10.48550/arXiv.2401.10166.

Liu Z, Lin Y T, Cao Y et al. 2021. Swin transformer: hierarchical vision transformer using shifted windows. *In*: 2021 IEEE/CVF International Conference on Computer Vision (ICCV). IEEE, Montreal, QC, Canada. p.9992-10002, https://doi.org/10.1109/ICCV48922.2021.00986.

Ma X P, Zhang X K, Pun M O. 2024. RS^{3}Mamba: visual state space model for remote sensing image semantic segmentation. *IEEE Geoscience and Remote Sensing Letters*, **21**: 6011405, https://doi.org/10.1109/LGRS.2024.3414293.

Pang J Z, Ren G B, Shi Q et al. 2021. Analysis of coral reef bleaching in Yongle Islands of Xisha from 2005 to 2018 based on sediment types change monitoring. *Marine Sciences*, **45**(6): 92-106, https://doi.org/10.11759/hykx20200729002. (in Chinese with English abstract)

Roelfsema C, Kovacs E, Ortiz J C et al. 2018. Coral reef habitat mapping: a combination of object-based image analysis and ecological modelling. *Remote Sensing of Environment*, **208**: 27-41, https://doi.org/10.1016/j.rse.2018.02.005.

Roelfsema C, Phinn S, Jupiter S et al. 2013. Mapping coral reefs at reef to reef-system scales, 10s-1000s km^2, using object-based image analysis. *International Journal of Remote Sensing*, **34**(18): 6367-6388, https://doi.org/10.1080/01431161.2013.800660.

Roelfsema C M, Lyons M B, Castro-Sanguino C et al. 2021. How much shallow coral habitat is there on the Great Barrier Reef? *Remote Sensing*, **13**(21): 4343, https://doi.org/10.3390/rs13214343.

Ruan J C, Li J C, Xiang S C. 2024. VM-UNet: vision mamba UNet for medical image segmentation. arXiv preprint arXiv:2402.02491, https://doi.org/10.48550/arXiv.2402.02491.

Wan J X, Ma Y. 2020. Multi-scale spectral-spatial remote sensing classification of coral reef habitats using CNN-SVM. *Journal of Coastal Research*, **102**(S1): 11-20, https://doi.org/10.2112/SI102-002.1.

Wan J X, Qin Z L, Cui X D et al. 2023. Seafloor habitat mapping by combining multiple features from optic and acoustic data: a case study from Ganquan Island, South China Sea. *IEEE Journal of Selected Topics in Applied Earth Observations and Remote Sensing*, **16**: 7248-7263, https://doi.org/10.1109/JSTARS.2023.3298472.

Wang L B, Li R, Zhang C et al. 2022. UNetFormer: a UNet-like transformer for efficient semantic segmentation of remote sensing urban scene imagery. *ISPRS Journal of Photogrammetry and Remote Sensing*, **190**: 196-214, https://doi.org/10.1016/j.isprsjprs.2022.06.008.

Wicaksono P, Aryaguna P A, Lazuardi W. 2019. Benthic habitat mapping model and cross validation using machine-learning classification algorithms. *Remote Sensing*, **11**(11): 1279, https://doi.org/10.3390/rs11111279.

Zhang C Y. 2015. Applying data fusion techniques for benthic habitat mapping and monitoring in a coral reef ecosystem. *ISPRS Journal of Photogrammetry and Remote Sensing*, **104**: 213-223, https://doi.org/10.1016/j.isprsjprs.2014.06.005.

Zhang F F. 2023. Research on Deep Learning Classification Method of Coral Reef Geomorphic Types based on Multi-Scale Remote Sensing. Inner Mongolia Normal University, Inner Mongolia. (in Chinese with English abstract)

Zhang F F, Hu Y B, Ma Y et al. 2024. GCU-Net: remote sensing classification method for coral reef geomorphology integrating geospatial cognition. *IEEE Geoscience and Remote Sensing Letters*, **21**: 5003805, https://doi.org/10.1109/LGRS.2024.3406681.

Zhao S J, Chen H, Zhang X L et al. 2024. RS-Mamba for large remote sensing image dense prediction. arXiv preprint arXiv:2404.02668, https://doi.org/10.48550/arXiv.2404.02668.

Zhu L H, Liao B C, Zhang Q et al. 2024a. Vision mamba: efficient visual representation learning with bidirectional state space model. arXiv preprint arXiv:2401.09417, https://doi.org/10.48550/arXiv.2401.09417.

Zhu Q F, Cai Y Z, Fang Y et al. 2024b. Samba: semantic segmentation of remotely sensed images with state space model. *Heliyon*, **10**(19): e38495, https://doi.org/10.1016/j.heliyon.2024.e38495.

Zou Y R, Lin M S, Wang H et al. 2006. Study on high resolution image classification for Dongsha Island based on fuse information. *Acta Oceanologica Sinica*, **28**(1): 56-61, https://doi.org/10.3321/j.issn:0253-4193.2006.01.008. (in Chinese with English abstract)